





Experimental study of entrainment behavior of debris flow over channel inflexion points

HU Kai-heng^{1,2}  <http://orcid.org/0000-0001-8114-5743>;  e-mail: khhu@imde.ac.cn

PU Li^{1,2,3}  <http://orcid.org/0000-0003-0591-4007>; e-mail: lipus9009@126.com

WANG Xie-kang⁴  <http://orcid.org/0000-0003-0065-404X>; e-mail: wangxiakang@scu.edu.cn

1 Key Laboratory of Mountain Hazards and Earth Surface Processes, Chinese Academy of Sciences, Chengdu 610041, China

2 Institute of Mountain Hazards and Environment, Chinese Academy of Sciences & Ministry of Water Conservancy, Chengdu 610041, China

3 University of Chinese Academy of Sciences, Beijing 100049, China

4 State Key Laboratory of Hydraulics and Mountain River Engineering, Sichuan University, Chengdu 610065, China

Citation: Hu KH, Li P, Wang XK (2016) Experimental study of entrainment behavior of debris flow over channel inflexion points. *Journal of Mountain Science* 13(6). DOI: 10.1007/s11629-015-3749-6

© Science Press and Institute of Mountain Hazards and Environment, CAS and Springer-Verlag Berlin Heidelberg 2016

Abstract: On-spot observation and field reconnaissance of debris flows have revealed that inflexion points in the longitudinal profile of a movable channel may easily become unstable points that significantly affect their entrainment behavior. In this study, small-scale flume experiments were performed to investigate the entrainment characteristics of debris flows over two types of inflexion points, namely, a convex point, which has an upslope gradient that is less than the downslope gradient; and a concave point, which has an upslope gradient that is greater than the downslope gradient. It was observed that when debris flowed over a convex point, the entrainment developed gradually and progressively from the convex point in the downstream direction, and the primary control factors were the slope gradient and friction angle. Conversely, when debris flowed over a concave point, the entrainment was characterized by impacting and impinging erosion rather than traditional hydraulic erosion, and the impingement angle of the flow significantly determined the maximum erosion depth and outflow exit angle. An empirical relationship between the topography change and the control

factors was obtained from the experimental data.

Keywords: Debris flow; Entrainment; Inflexion points; Erosion; Impingement angle

Introduction

Debris flows entraining massive sediments while flowing down steeply hillslopes or channels may become exceptionally mobile and destructive (Hung 2005). The entrainment factors that may increase the magnitude of the debris flow and substantially amplify its destructive power include the mobilization of discrete landslides, coalescence of erosional rills, and exceptional concentration of the surface water (Cannon et al. 2001; Wang et al. 2003; Godt and Coe 2007; Coe et al. 2008). For example, the Tsing Shan debris flow in 1990, which is considered to be the largest debris flow event in Hong Kong, had a small initial slip of 400 m³ but enlarged to a final volume of 20,000 m³ through the entrainment of colluvium along its flow path (King 1996). A giant debris flow that developed in

Received: 23 February 2016
Accepted: 14 April 2016

the Wenjia catchment of China on 13 August 2010 transported about 3 million m³ of sediment, most of which originated from the 2008 Wenchuan earthquake-induced landslides, to the downstream river (Tang et al. 2012).

Some mechanisms of debris-flow entrainment have been proposed. Sassa (1985) suggested that loading by overriding debris flows could transiently increase the pore pressure in saturated bed sediments, and that an excess pore pressure might nearly liquefy the bed, thereby significantly reducing the bed sediment shear strength and facilitating entrainment. Takahashi (1978, 1991) proposed that saturated bed sediment failed as a whole and groundwater pressure in the sediment was in equilibrium with the sloping water table in an overriding debris flow, and there was thus no transient development of excess pore pressure. Hungr (2005) derived a modified equation from Takahashi's equation based on the observation that a steady seepage condition could hardly be achieved within the short duration of the passage of a surge peak. Iverson et al. (2011) performed debris flow flume tests and observed positive feedback and momentum growth when a debris flow entrained wet bed sediments. Iverson (2012) considered the mass and momentum exchange between a debris flow and an underlying sediment layer, and suggested that the entrainment rates satisfied a jump condition involving shear traction and velocity discontinuities at the flow bed boundary.

With regard to the calculation of the entrainment rate, Takahashi et al. (1986) suggested the concept of the equilibrium sediment concentration and used it to evaluate the erosion entrainment rate, while Egashira et al. (2001) proposed an erosion rate formula based on the assumption that the bed slope always adjusts to its equilibrium state when a debris flow occurs over an erodible bed. However, Suzuki et al. (2009) found some problems in the application of these formulas under highly unsteady conditions, and proposed a new entrainment rate equation based on the assumption that the difference between the amounts of sediment in the debris flow and the equilibrium state controls the erosion and deposition. Brufau et al. (2000) encountered a paradox in the use of Egashira's equation to calculate the entrainment rate on an adverse slope,

namely, that the equation always tends to produce deposition even when erosion should occur. They thus introduced the slope of the energy line and obtained ideal results even for adverse slopes.

It is obvious from the foregoing that the entrainment process of a debris flow is closely related to the topographic conditions of the channel. Shied et al. (1996) proposed that the process of deposition within the range of the abrupt variation of the bed inclination was non-equilibrium, and that the local concentration could not be estimated by Takahashi's equilibrium equation. Hence, in the present study, we investigated the effects of the topographic inflexion points along the channel on the entrainment behavior of a debris flow. Such inflexion points are mainly formed by plentiful loose material, which might have originated from landslides and avalanches induced by intense seismic shaking and post-seismic rainfalls (Lin et al. 2006; Koi et al. 2008; Lin et al. 2008; Khattak et al. 2010). The super strong erosion by debris flows happened at these inflexion points such as Zhouqu event of August 8, 2010 and Qingping event of August 13, 2010 in the western China greatly reduced the stability of channel beds and rockfall dams, and hence increased debris-flow magnitude (Tang et al. 2011; Hu et al. 2012; Cui et al. 2013)(Figure 1).

As shown in Figure 2, the abrupt deposition of loose material in the channel changes the original bed morphology, resulting in an irregular distribution of inflexion points, where the upslope gradient is not equal to the downslope gradient. This alternation of steep and gentle slopes in the longitudinal profile of the channel may easily cause the inflexion points to become unstable points where strong erosion is initiated. As described by Tang et al. (2012), the thick accumulations of loose landslide material in the Wenjia mainstream reshaped the channel topography and made it prone to erosion and remobilization into debris flows during periods of intense and prolonged rainfall. The above-mentioned theories and equations of debris flow entrainment involve various factors that affect the entrain process, including the sediment pore pressure and water content and the changes in mass and momentum. However, the effects of external topographic conditions such as inflexion points were rarely considered in the development of the theories and equations.

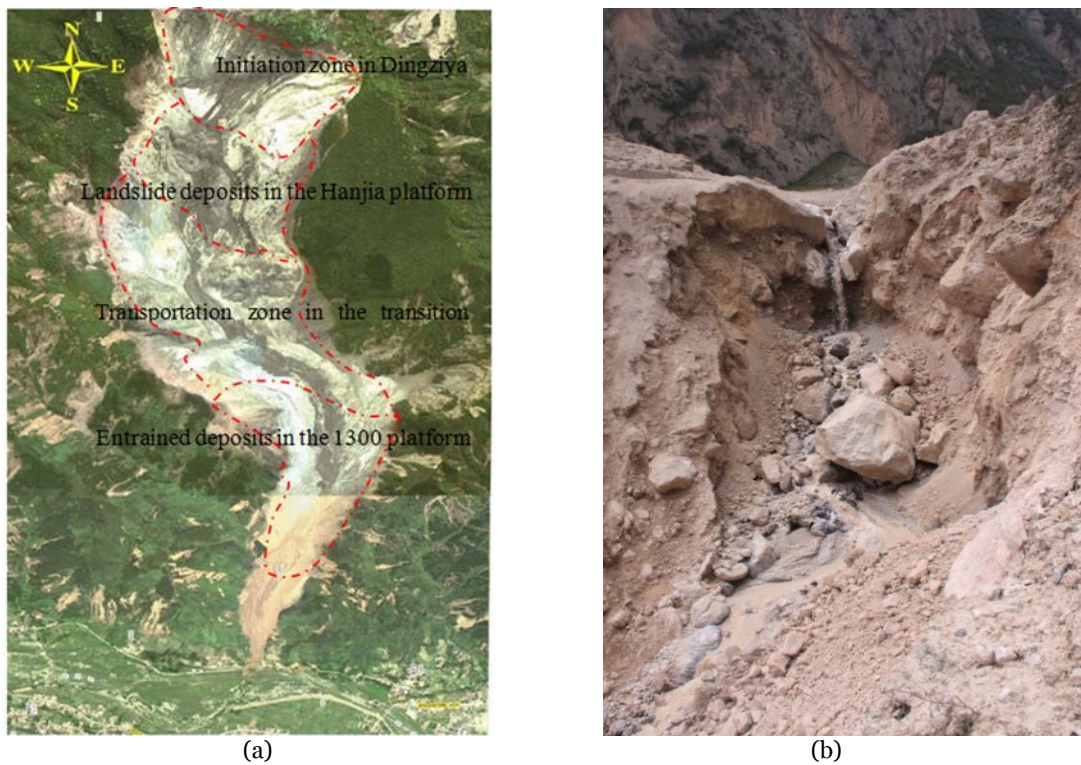


Figure 1 Study area. (a) Aerial photograph, taken on May 18, 2008, providing an overview of the debris flow channel of the Wenjia catchment with four obvious slope-discontinuous sections; (b) A photograph of rock-fill dam formed in the Sanyanyu valley in Zhouqu area.

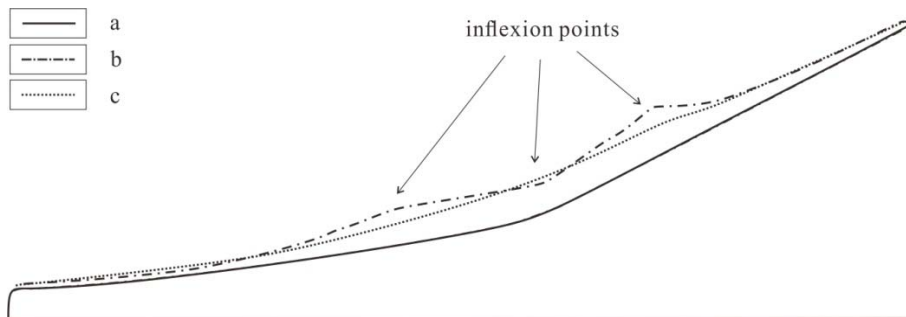


Figure 2 Sketch of topographic morphology of debris flow channel. a: original channel profile, b: channel profile reshaped by fresh-born loose material, with topographic inflexion points, c: envisaged channel profile after entrainment by subsequent debris flow events.

In the present study, we designed and performed flume experiments to investigate the entrainment process of debris flows at topographic inflexion points. From Figure 1, we identified two types of topographic inflexion points, namely, a convex point, which is characterized by transition from a gentle slope to a steep slope; and a concave point, which is characterized by a transition from a steep slope to a gentle slope. We examined the difference between the entrainment mechanisms and the two types of inflexion point.

1 Experimental Setup and Procedure

The experiments were performed in an elaborately constructed flume in the Jiangjia gully, Yunnan China. The experimental setup included a narrow flume between armored glass walls spaced at 0.3 m. The inclination of the 6-m long and 1-m high planar flume θ_0 was fixed to 10° . To investigate the effect of the topographic inflexion points on the erosion features of the debris flow, we designed an erodible bed composed of three topography shapes

with transition angle α_0 values of 15° , 25° , and 35° respectively (Figure 3). In each experiment, the upstream inflexion point was convex and the downstream inflexion point was concave. The different transition angles represented different curvatures of the topographic convex and concave points. The erodible bed was divided into three main parts. The upstream sediment bed was set up parallel to the flume bed and had a thickness of 0.6 m; the middle part was inclined at the transition angle and its thickness varied linearly from 0.6 m to 0.2 m; and the downstream part was also set up parallel to the flume bed and had a thickness of 0.2 m. In Figure 3, α_0 denotes the transition angle of the sediment bed. A debris mixture of volume 0.5 m^3 was released from a hopper. The debris material, which was uniformly mixed with water, was the same as that of the sediment bed. The bulk density of the mixture was chosen between 1400 and 1800 N/m^3 . In order to generate a regular inflow, we designed a 2-m long fixed-bed section OA between the hopper outlet and the erodible-bed section AB . As shown in the Figure 3. When the released debris flow passing through this section, the turbulence and rolling wave intensity of debris flow was suppressed to some extent and hence the overall flow velocity tends to be relatively stable and uniform.

The grain size distribution curves show in

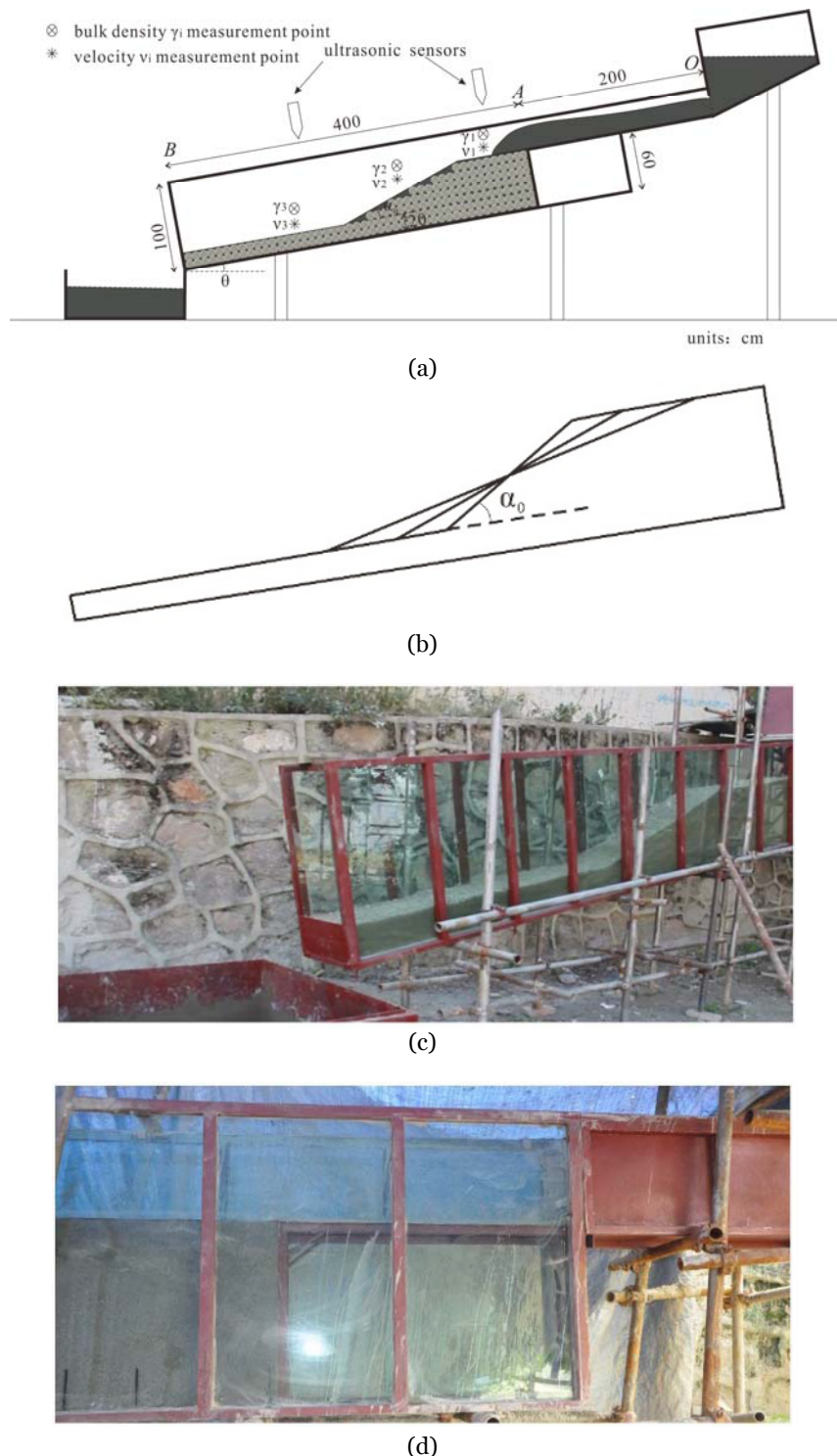


Figure 3 Experimental setup: (a) schematic of the experimental facility; (b) shape of the erodible bed section AB with different transition angles; (c) Photo of erodible bed section AB ; (d) Photo of fixed-bed section OA .

Figure 4. The maximum diameter d_{max} and the median diameter d_{med} of sediment composition in the experiments are 1.5 cm and 0.30 cm

respectively. The erodible bed was composed by disturbed soils with the bulk density $\gamma_{bed} = 1810 \text{ N/m}^3$, and the mean friction angle $\varphi = 30^\circ$. The resistance of the bed materials to debris-flow entrainment largely depends on the soil compactness and shear strength.

Another important factor that affects the sediment entrainment is the volumetric water content. Iverson et al. (2011) found that a high positive pore pressure was developed during the entraining of wet bed sediments and that the increased pore pressure facilitated progressive scouring of the bed, reduced basal friction, and instigated feedback. A positive feedback was found to increase the flow velocity, mass, and momentum of wet bed sediments, whereas a negative feedback decreased the flow velocity and momentum of dry bed sediments. In our experiments, the bed water content was $6 \pm 1\%$, which is relatively low. We therefore assumed that the pore pressure during the entrainment process could be ignored, and that the dominant control factor was the sediment friction angle.

The experiments were performed for 36 cases comprising different bed material diameters, sediment diameters of debris flows, and transition angles. The bulk density of the mixture released from the hopper was stochastically controlled within the range of diluent debris flows. To estimate the real-time variation of the sediment-water mixture discharge from the channel inlet, three controlled experiments were performed using a designed planar sediment bed. One of the measured debris flow height data is shown in Figure 5, from which the release duration of the mixture from the hopper can be determined to be about 6 s. The peak flow height of 14 cm denoted by the blue line in Figure 5, was approximately maintained during the first 4 s, after which the velocity decreased to zero within the next 2 s. In view of the transient duration of the release of the debris mixture, we propose the flow-front velocity of the mixture during the entire duration of the experiment. The entire entrainment process was assumed to mainly occur during the 4 s duration when the peak sediment-water mixture discharge was maintained as depicted by the red dashed line box in Figure 5.

As shown in Figure 3, two ultrasonic sensors were installed before the upper transition angle

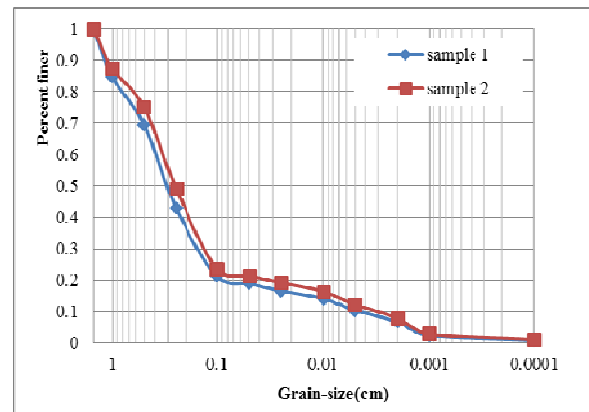


Figure 4 Grain size distribution curves of two experimental samples.

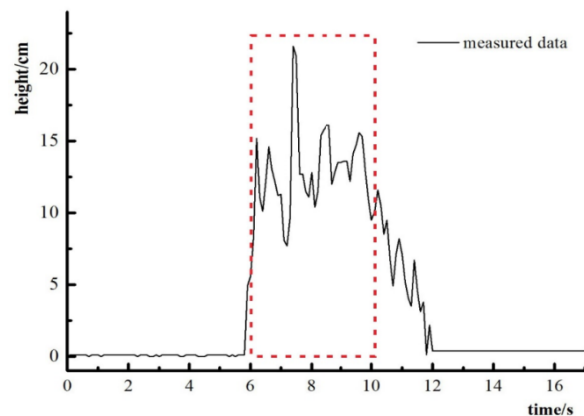


Figure 5 Measured flow height data for the controlled experiments.

and after the lower transition angle, respectively, to record the evolving flow height h of the released debris as it flowed down the flume, at a rate of 30 Hz. Considering that the sediment bed was erodible, the real-time erosion rates at the flow height measurement points was determined from the side-view recording of a digital video camera and used to calibrate the flow height data. Because the debris flows changed their volume and altered their features by the entrainment of the sediment bed along the uneven path, we examined the variation of the debris flow bulk density along the path by sampling before the upper transition angle, after the lower transition angle, and in the middle of the steep slope between the two transition angles, as shown in Figure 3. The bulk densities determined at the foregoing points were denoted by γ_1, γ_2 and γ_3 , respectively. The flow front velocity was determined by tracking the flow with the digital video camera and analyzing the images at

the three topographic inflexion sites. The determined velocities in the downstream direction at the three sites were respectively denoted by v_1, v_2 and v_3 , from. The erosion depth in the sediment bed z_i , was determined by point gauges immediately after the debris flow supply was stopped. The measurements were taken at 10 cm intervals along the entrainment path. All the control variables and measurements are presented in Table 1 below.

2 Experimental Results

An analysis of the measured data revealed that the erosion rate of the sediment bed and the post-

experiment bed morphology were mainly determined by the transition angle. The pre- and post-experiment bed morphologies for different transition angles are shown in Figure 6.

To eliminate the variation of the erosion due to the varying bulk density, we averaged the measured erosion depths for each series of experiments with the same transition angle. The average values are presented in Figure 7.

The different transition angles correspond to different curvatures of the topographic inflexion points. From Figures 6 and 7, it can be determined that the evolutions of the erodible bed morphology at the convex and concave points tend to differ.

Table 1 Control variables and measured data of the experiments

Run	$\alpha_0(^{\circ})$	d_{med} (cm)	γ_{bed} (N/m ³)	$\varphi(^{\circ})$	γ_1	γ_2	γ_3	v_1	v_2	v_3	V_e (m ³)
					(N/m ³)			(m/s)			
1	15	0.3	1810	30	1522	1620	1660	7.2	8.25	6.99	0.059
2	15	0.3	1810	30	1714	1781	1852	8.16	7.65	8.08	0.082
3	15	0.3	1810	30	1530	1575	1798	8.22	8.79	9.13	0.083
4	15	0.3	1810	30	1547	1606	1702	8.16	8.02	8.06	0.081
5	15	0.3	1810	30	1788	1844	1877	8.48	7.59	7.61	0.077
6	15	0.3	1810	30	1481	1595	1683	8.38	8.18	8.81	0.097
7	15	0.3	1810	30	1511	1615	1706	7.57	7.66	9.47	0.080
8	15	0.3	1810	30	1572	1640	1700	8.43	7.41	8.22	0.094
9	15	0.3	1810	30	1546	1581	1764	7.94	7.65	9.22	0.102
10	15	0.3	1810	30	1716	1791	1842	7.72	7.94	8.31	0.087
11	15	0.3	1810	30	1589	1622	1755	8.45	8.77	8.75	0.104
12	15	0.3	1810	30	1645	1746	1799	7.81	8.02	8.45	0.090
13	25	0.3	1810	30	1613	1714	1794	6.72	8.57	7.26	0.069
14	25	0.3	1810	30	1523	1620	1735	6.73	6.81	7.72	0.075
15	25	0.3	1810	30	1555	1615	1708	7.53	8.18	9.74	0.062
16	25	0.3	1810	30	1547	1631	1699	7.13	7.49	8.73	0.066
17	25	0.3	1810	30	1682	1713	1841	7.47	8.29	8.73	0.069
18	25	0.3	1810	30	1338	1384	1417	8.52	8.74	0.23	0.083
19	25	0.3	1810	30	1573	1676	1779	7.44	7.6	9.35	0.067
20	25	0.3	1810	30	1644	1756	1849	6.79	8.11	8.48	0.083
21	25	0.3	1810	30	1486	1541	1615	7.85	8.32	0.6	0.092
22	25	0.3	1810	30	1678	1815	1944	7.32	7.43	8.4	0.076
23	25	0.3	1810	30	1575	1663	1751	8.81	7.63	9.72	0.093
24	25	0.3	1810	30	1700	1809	1910	7.32	7.74	8.63	0.079
25	35	0.3	1810	30	1626	1701	1749	6.93	7.66	6.91	0.072
26	35	0.3	1810	30	1526	1621	1719	7.14	7.34	6.96	0.048
27	35	0.3	1810	30	1622	1691	1758	7.97	7.66	8.72	0.069
28	35	0.3	1810	30	1537	1653	1743	8.08	7.33	6.56	0.050
29	35	0.3	1810	30	1679	1839	1903	7.47	7.64	7.84	0.059
30	35	0.3	1810	30	1369	1468	1644	8.81	7.89	6.67	0.075
31	35	0.3	1810	30	1455	1543	1595	8.15	7.95	7.34	0.061
32	35	0.3	1810	30	1544	1608	1644	6.95	8.33	4.88	0.074
33	35	0.3	1810	30	1544	1651	1793	8.62	7.72	8.43	0.084
34	35	0.3	1810	30	1663	1749	1819	7.6	7.86	7.71	0.067
35	35	0.3	1810	30	1474	1556	1599	8.79	7.99	6.65	0.085
36	35	0.3	1810	30	1517	1608	1671	8.56	8.16	7.57	0.080

Notes: The total erosion amount V_e for each experiment was calculated using $V_e = \sum_{i=1}^n V_{ei} = \sum_{i=1}^n 0.5 * (z_i + z_{i+1}) * l_i * b_i$, where n is the measurement point number, z_i and z_{i+1} are the erosion depths at two adjacent measurement points, l_i is the distance between the two adjacent points, and b_i is the width of the flume.

When the debris flow passed over the topographic convex point, it significantly affected the morphology evolution of the downstream steep slope. The entrainment process in this section started at the convex point and progressively propagated in the downward direction, layer-by-layer. During its evolution, the entrainment behaved like an “induced” mass erosion, as in a highly developed localized landslide or avalanche. When the overriding debris flow passed over the convex point, it applied a force on the erodible material on the steep slope. The entrainment process was mainly controlled by the slope angle, which determined the localized slip energy and the bed material stability, which acted as an anti-slip factor.

When the debris flowed over the topographic concave point, the erosion depth in the downstream platform was obviously greater in the section with the steeper transition angle. When the flow transited from the steep slope to the gentle slope, the collision of the debris mixture was severe and the impact affected the lower erodible bed. The result was the formation of a rather deep erosion hole, which led to an abrupt termination of the erosion beyond the downstream boundary of the hole. When the debris flow transited from the steep slope to the gentle slope, the transient dynamic collision and impact erosion became extremely prominent. The relatively dry and loose portions of the sediment bed material also facilitated abrasive wear, surface fatigue wear, and front plowing. Under these conditions, the entrainment characteristics of the debris flow largely depended on the physical properties and strength of the sediment bed material.

The inflexion points in the channel topography

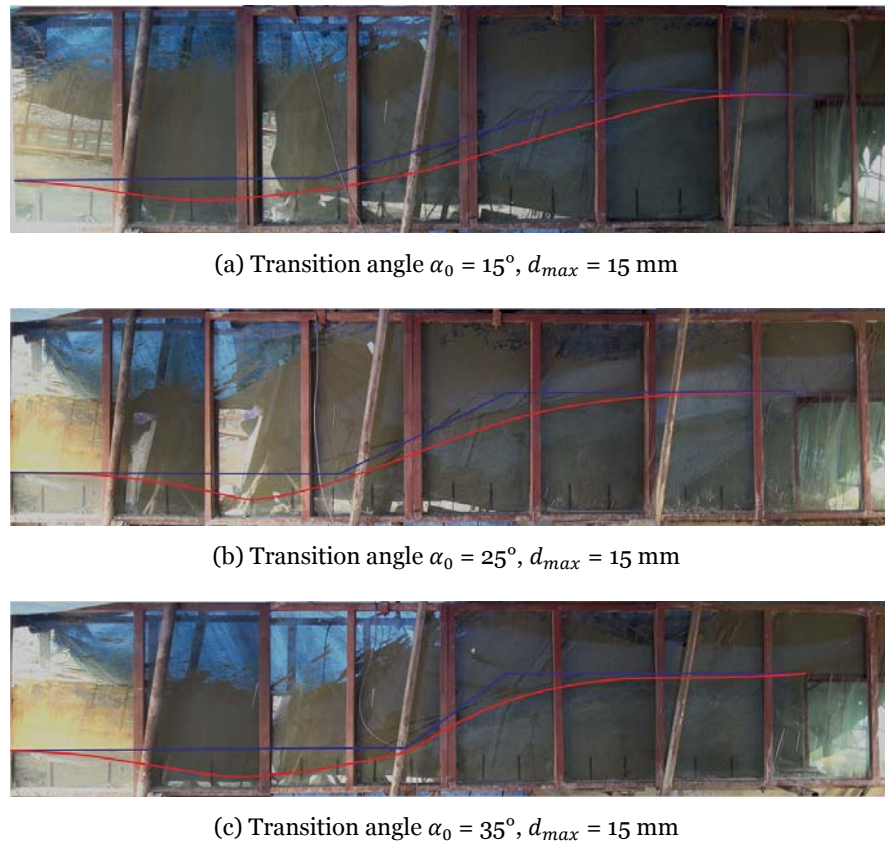


Figure 6 Pre- and post-experiment bed morphologies for different transition angles. The blue and red lines respectively represent the pre- and post-experiment bed morphologies.

made the entrainment of the erodible bed quite elusive. Figure 8 shows the detailed evolution of the bed morphology.

The initial sediment bed was divided into three sections: sections OA , AB , and BC . With regard to the inflexion points produced by the irregular heaping of loose material in the debris flow channel, the present experiments were used to investigate how the entrainment characteristics in sections AB and BC were respectively affected by the transition angles $\angle OAB$ and $\angle ABC$, which respectively correspond to convex and concave points. The bed morphology after the experiment is indicated by the dotted line in Figure 8, where the maximum erosion depth AL in section AB is denoted by E_{m1} and MN in section BC is also denoted by E_{m2} . The maximum erosion depth MN and AL were measured perpendicularly to the line BC and AB respectively, and the erosion depths E_{i1} and E_{j1} were measured perpendicularly to the line AB . The shape of the post-experiment sediment bed is divided into three sections: sections OL , LN , and

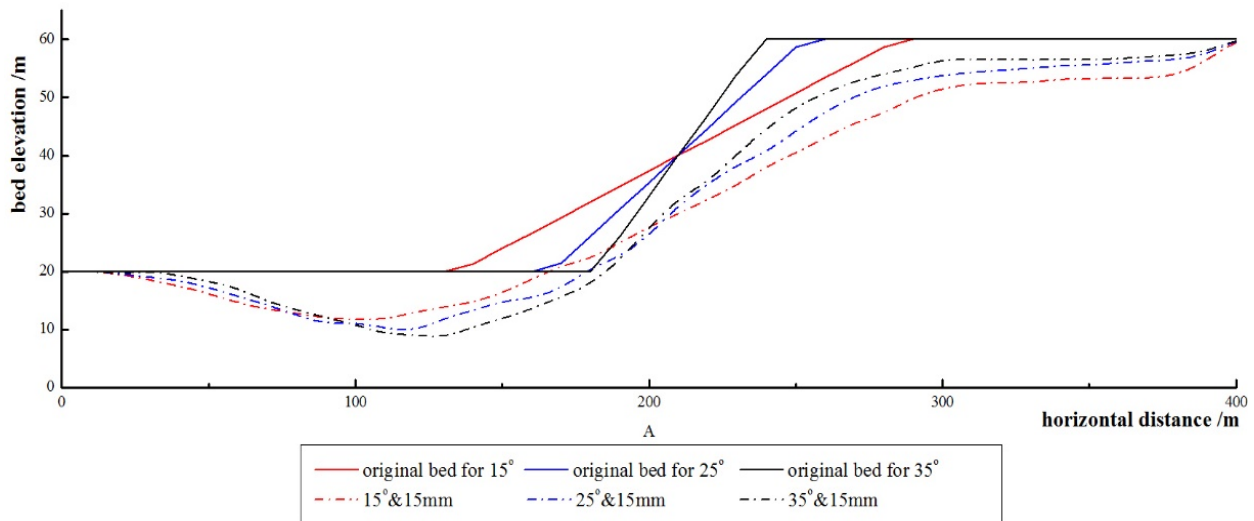


Figure 7 Post-experiment bed morphologies for different transition angles $\alpha_0=15^\circ, 25^\circ, 35^\circ$. The solid coloured lines denote the Post-experiment bed morphologies and the dashed ones denote the Post-experiment bed morphologies.

NC. The initial slope incline of section OA and section AB are denoted by θ_0 and α_1 , where $\alpha_1 = \alpha_0 + \theta_0$. While the post-experiment slope inclines of section OA and section AB are denoted by θ_1 and α_1 , respectively. The pre- and post-experiment slope inclines of section BC are respectively denoted by θ_0 and β . When the tangent line is below the horizontal line, β is negative; otherwise, it is positive. In Figure 8, β is negative. α_2 and β were respectively determined by linear fitting within sections LN and NC. The average value of α_1 and α_2 was denoted as α and the average value of θ_0 and θ_1 was denoted as θ . To facilitate analysis of the bed morphology evolution and entrainment process, we represented the pre- and post-experiment incline angles relative to the

horizontal of the respective sections, as shown in Figure 9.

Figures 7 and 8 can be used to determine the variation of the erosion depth $(E_{i1} - E_{j1})/l_1$ with the change in the topography incline angle $\tan(\alpha_2 - \alpha_1)$, in section AB. Both variables are closely correlated with the initial bed slope α of section AB and the debris flow physical parameters γ_1, v_1 and h_1 . We could also determine the variation of the erosion depth $(E_{i2} - E_{j2})/l_2$, with the change in the topography incline angle $\tan(\theta_0 - \beta)$, in section BC. Both variables here are also closely correlated with the impact angle of the debris flow (mostly equal to the initial bed slope α_1 of section AB) and the debris flow physical parameters γ_2, v_2 and h_2 .

The experimental parameters and measured variables are presented in Table 2.

3 Analysis

3.1 Features of entrainment when debris flows over convex point

To examine the topographic convex points, we focused on the entrainment characteristics in section AB. The considered pre-experiment

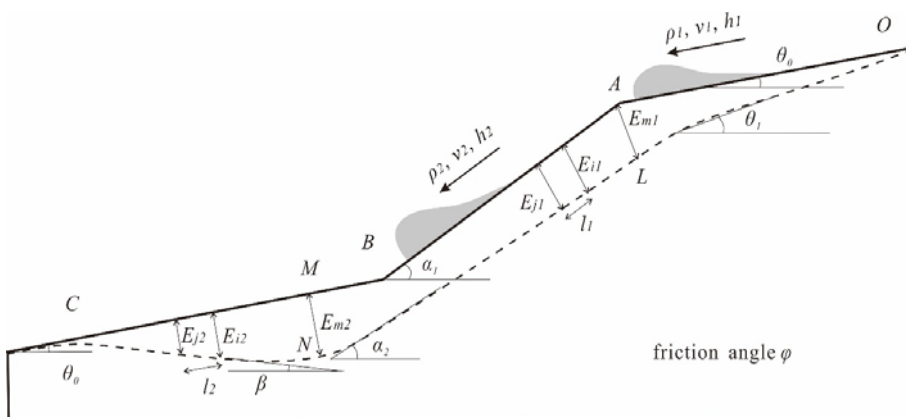


Figure 8 Schematic of the bed morphology evolution. The initial erodible bed can be divided into three parts: section OA, section AB and section BC. The post-experiment bed profile also consists of three parts: section OL, section LN and section NC.

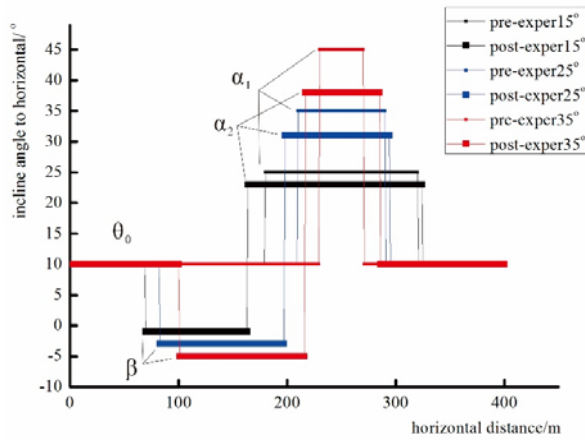


Figure 9 Pre- and post-experiment incline angles relative to the horizontal of the respective sections.

incline angles of section *AB* were 25°, 35°, and 45°, respectively. The following erosion rate equations of debris flow proposed by Takahashi et al. (1986) were employed:

$$\frac{E}{v} = \zeta \frac{c_e - c}{c_s - c_e} \frac{h}{d} (E \geq 0) \quad (1)$$

$$\frac{E}{v} = \eta (c_e - c) \frac{h}{d} (E < 0) \quad (2)$$

It can be deduced from the above equations that the erosion rate is mainly related to the value of h/d and the debris flow velocity v , which is determined by the sediment concentration. In our study, we introduced the term γ_1/γ_{bed} , where γ_1 is the unit weight of the debris flow in the upstream section *OA*, and γ_{bed} is the unit weight of the remolded sediment bed. These terms can be used to partly describe the compactness and strength of the erodible bed material.

As noted above, the water content of the material of the sediment bed was as low as 6%±1%, for which reason we assumed that the key determinant of the strength of the sediment bed in section *AB* was the sediment friction angle. Considering the rather steep incline of section *AB* and the strong dynamic effect of the debris flow passing through the inflexion point *A*, the mass erosion played a vital role in the evolution of the sediment bed erosion. We considered the average value of original and post-experiment bed incline angle α as the slip factor, which is a measure of the overall instability of an erodible bed on a steep slope. In addition, the friction angle φ of the bed material was considered as the anti-slip factor,

which is a reflection of the strength and stability of a sediment bed. The instability factor of the slope material, $\tan\alpha/\tan\varphi$ was introduced and assumed to be positively correlated with the intensity of the mass erosion. When the slope angle was significantly smaller than the friction angle, the difference between the two had little effect on the mass erosion process. This is in agreement with the generally accepted thought that hydraulic erosion is more dominant than mass erosion in a relatively gentle channel. However, the intensity of mass erosion is significantly increased when the slope angle is larger than the friction angle. This is because the steeper incline increases the sediment instability. We thus came up with the erosion depth variation $(E_{i1} - E_{j1})/l_1$ along the path and used it to describe the intensity of the mass erosion on the steep slope. The value of the variation reflects the rate of change of the slope inclination from steep to gentle, and was found to be equal to the change in the topography incline angle, given by $\tan(\alpha_2 - \alpha_1)$. Similarly, we assume that the maximum erosion depth E_{m1} of section *AB* denoted as AL , mainly depend on the instability factor of the slope material $\tan\theta/\tan\varphi$. As an analogy of the erosion rate equation of Takahashi, we propose the following empirical erosion relationship:

$$E_{m1} = a * \frac{h_1}{d_m} * \frac{\gamma_1}{\gamma_{bed}} * v_1 * f_1 \left(\frac{\tan\theta}{\tan\varphi} \right) \quad (3)$$

$$\tan(\alpha_2 - \alpha_1) = \frac{E_{i1} - E_{j1}}{l_1} = b * \frac{h_1}{d_m} * \frac{\gamma_1}{\gamma_{bed}} * v_1 * f_2 \left(\frac{\tan\alpha}{\tan\varphi} \right) \quad (4)$$

The terms E_{m1} , $(E_{i1} - E_{j1})/l_1$, h_1/d_m , γ_1/γ_{bed} , and v_1 in the above equation can be calculated from the measured parameters in Table 2. The term a and b are experimental coefficients yet to be determined. To determine the proper form of the function f_1 and f_2 , we applied a simple formula deformation tactic, which gave

$$E = \frac{E_{m1}}{\frac{h_1}{d_m} * \frac{\gamma_1}{\gamma_{bed}} * v_1} = a * f_1 \left(\frac{\tan\theta}{\tan\varphi} \right) \quad (5)$$

$$F = \frac{\frac{E_{i1} - E_{j1}}{l_1}}{\frac{h_1}{d_m} * \frac{\gamma_1}{\gamma_{bed}} * v_1} = b * f_2 \left(\frac{\tan\alpha}{\tan\varphi} \right) \quad (6)$$

The variable E and F on the left side of Eqs.(5-

Table 2 Experimental parameters and measured variables

Run	h_1 (cm)	γ_1 (N/m ³)	v_1 (m/s)	θ (°)	E_{m1} (cm/s)	ΔE_{ij1} (cm/s)	h_2 (cm)	γ_2 (N/cm ³)	v_2 (m/s)	α (°)	Fr	E_{m2} (cm/s)	ΔE_{ij2} (cm/s)
1	11.1	1522	7.2	24.6	1.8	0.0027	14.1	1620	8.25	24.6	48.3	1.9	0.0231
2	11.9	1714	8.16	24.0	2.7	0.0087	15.1	1781	7.65	24.0	38.8	2.2	0.0272
3	12.4	1530	8.22	24.5	2.2	0.0039	14.6	1575	8.79	24.5	52.9	2.1	0.0268
4	12.4	1547	8.16	24.3	2.1	0.0053	15.9	1606	8.02	24.3	40.5	2.4	0.0276
5	11.9	1788	8.48	24.3	2.3	0.0055	15.5	1844	7.59	24.3	37.2	2.0	0.0247
6	12.8	1481	8.38	24.1	2.8	0.0079	14.4	1595	8.18	24.1	46.5	2.3	0.0265
7	11.7	1511	7.57	24.4	2.2	0.0048	14.9	1615	7.66	24.4	39.4	2.1	0.0258
8	11.2	1572	8.43	24.1	2.7	0.0077	15.8	1640	7.41	24.1	34.8	2.3	0.0256
9	13.9	1546	7.94	23.9	3.0	0.0091	15.3	1581	7.65	23.9	38.3	2.3	0.0253
10	12.6	1716	7.72	24.2	2.5	0.0066	14.9	1791	7.94	24.2	42.3	2.2	0.0258
11	13.2	1589	8.45	23.9	3.1	0.0092	15	1622	8.77	23.9	51.3	2.3	0.0257
12	12.3	1645	7.81	24.2	2.6	0.0070	16.1	1746	8.02	24.2	40.0	2.2	0.0257
13	12.8	1613	6.72	31.5	2.9	0.0298	15.3	1714	8.57	31.5	48.0	2.6	0.0286
14	12.4	1523	6.73	32.3	2.7	0.0236	15.2	1620	6.81	32.3	30.5	2.5	0.0276
15	12.4	1555	7.53	31.9	2.8	0.0263	15.5	1615	8.18	31.9	43.2	2.5	0.0286
16	12.9	1547	7.13	31.5	3.1	0.0306	15.3	1631	7.49	31.5	36.7	2.6	0.0291
17	12.5	1682	7.47	31.9	2.8	0.0269	14.5	1713	8.29	31.9	47.4	2.6	0.0286
18	12.6	1338	8.52	31.5	3.4	0.0304	16.1	1384	8.74	31.5	47.4	2.7	0.0275
19	13.1	1573	7.44	31.8	2.9	0.0277	14.9	1676	7.6	31.8	38.8	2.6	0.0290
20	13.7	1644	6.79	31.4	3.4	0.0311	14.7	1756	8.11	31.4	44.7	2.7	0.0275
21	11.7	1486	7.85	31.3	3.6	0.0321	16.3	1541	8.32	31.3	42.5	2.7	0.0266
22	12.7	1678	7.32	31.6	3.1	0.0291	16.4	1815	7.43	31.6	33.7	2.6	0.0280
23	12.2	1575	8.81	31.2	3.7	0.0327	15.9	1663	7.63	31.2	36.6	2.7	0.0267
24	13.1	1700	7.32	31.5	3.2	0.0300	15.2	1809	7.74	31.5	39.4	2.6	0.0277
25	13.1	1626	6.93	38.4	3.5	0.0583	16	1701	7.66	38.4	36.7	3.3	0.0333
26	12	1526	7.14	38.1	3.5	0.0608	16.1	1621	7.34	38.1	33.5	2.5	0.0318
27	12	1622	7.97	36.7	4.0	0.0743	15.3	1691	7.66	36.7	38.4	3.0	0.0332
28	12.9	1537	8.08	39.4	3.2	0.0640	15.2	1653	7.33	39.4	35.3	2.7	0.0344
29	11.8	1679	7.47	38.0	3.6	0.0618	14.6	1839	7.64	38.0	40.0	2.8	0.0330
30	12.3	1369	8.81	37.5	4.1	0.0663	16.2	1468	7.89	37.5	38.4	2.9	0.0320
31	13.2	1455	8.15	37.9	3.6	0.0626	15.7	1543	7.95	37.9	40.3	2.9	0.0333
32	12.7	1544	6.95	37.9	4.0	0.0627	14.6	1608	8.33	37.9	47.5	2.9	0.0322
33	12.3	1544	8.62	37.3	4.3	0.0683	15.5	1651	7.72	37.3	38.5	3.0	0.0314
34	11.9	1663	7.6	37.9	3.8	0.0633	15	1749	7.86	37.9	41.2	2.9	0.0327
35	12.5	1474	8.79	37.3	4.3	0.0680	15.9	1556	7.99	37.3	40.2	3.0	0.0315
36	12.9	1517	8.56	37.5	4.2	0.0664	14.4	1608	8.16	37.5	46.2	3.0	0.0316

Notes: The debris flow heights h_1 and h_2 were determined by ultrasonic sensors, and γ_1, γ_2, v_1 , and v_2 are the same as in table 1. α_2 is the average of the pre- and post-experiment slope angles of section AB; $\theta = (\theta_0 + \theta_1)/2$, $\alpha = (\alpha_1 + \alpha_2)/2$. Fr is the Froude number of the debris-flow when passing through the downstream transition angle, given by $Fr = v_2^2/gh_2$. E_{m1} and E_{m2} are respectively the average of the maximum erosion depth MN in section BC and AL in section AB over 4 s. $\Delta E_{ij1} = (E_{i1} - E_{j1})/l_1$. $\Delta E_{ij2} = (E_{i2} - E_{j2})/l_2$.

6) are determined by the independent factor $\tan\theta/\tan\varphi$ from the graph in Figure 10 and $\tan\alpha/\tan\varphi$ from the graph in Figure 11 respectively.

From Figure 10 and 11, it was determined that $a = 0.0494$, b contains the coefficient E^{-6} and the index 4.168. The former is dimensionless while the latter has the dimension m^{-1} . This experimental coefficient, which has the dimension m^{-1} , is an indication of the erosion depth variation of the sediment bed along the debris flow path. It is also a measure of the mass erosion intensity and of the effect of planation at the convex point. To eliminate experimental errors, we assumed the coefficient to be a derived first-order exponential function. Our

proposed erosion equation thus becomes

$$E_{m1} = 0.05 * \frac{h_1}{d_m} * \frac{\gamma_1}{\gamma_{bed}} * v_1 * \frac{\tan\theta}{\tan\varphi} \tag{7}$$

$$\tan(\alpha_2 - \alpha_1) = \frac{E_{i1} - E_{j1}}{l_1} = E^{-6} * \frac{h_1}{d_m} * \frac{\gamma_1}{\gamma_{bed}} * v_1 * e^{4.618 * \frac{\tan\alpha}{\tan\varphi}} \tag{8}$$

3.2 Entrainment features when debris flows over concave point

To examine the topographic concave point at the transition from the gentle slope to the steep slope, we focused on the entrainment characteristic in section BC. Considering the low water content of

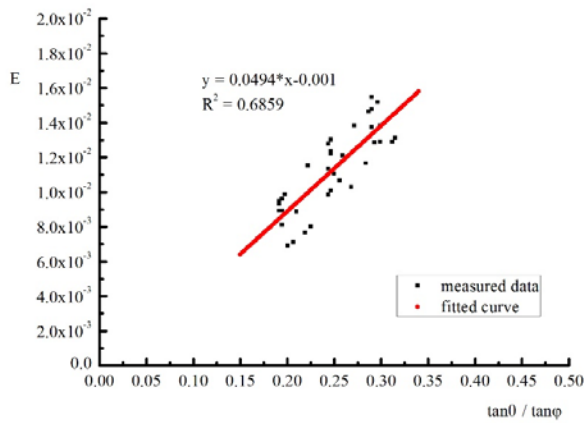


Figure 10 E as a function of $\tan\theta/\tan\varphi$.

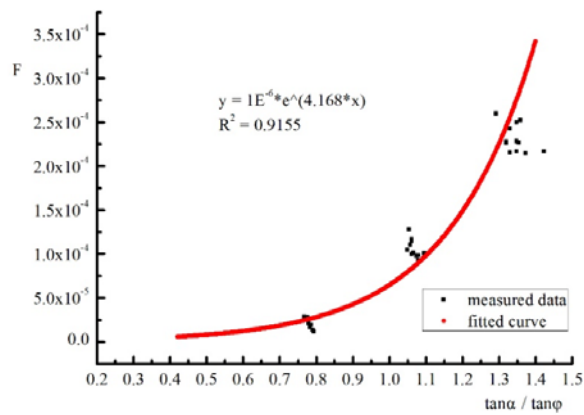


Figure 11 F as a function of $\tan\alpha/\tan\varphi$.

the sediment bed material and the fact that the liquid phase in the debris flow hardly permeated the bed layer within the very short experiment duration, we treated the debris flow over the sediment bed as a single-phase flow. Based on our intensive experimental observation and thorough analysis of the measured data, we concluded that, when the debris flow encountered the topographic concave point, the erosion of the downstream erodible bed was mainly controlled by instant impact erosion, which acted more like a jet impingement. Speaking about jet impingement, Rajaratnam (1981, 2003) used the densimetric Froude number to describe the characteristic features of a bed scoured by plane turbulent wall jets, and proposed that the velocity and thickness of the jet, the density of the eroding fluid, and the critical shear stress of the bed soil were the control factors of the profiles of the scoured hole. Beltaos (1973) considered the effects of the obliqueness, namely, the impingement of the jet at an arbitrary angle other than 90° . He suggested that, in addition to the jet velocity, the impingement angle

also significantly affected the position and maximum depth of the hole eroded in the bed.

As in the analysis of section AB , we considered the term h/d , debris flow velocity v , and term γ_2/γ_{bed} as the factors that affect the erosion process in the gently sloping section BC . The jet impingement effect was also adopted, and the impingement angle was considered as the primary determinant of the geometrical morphology of the erosion hole in section BC . We also posited that the maximum depth E_{m2} of the erosion hole was proportional to the vertical downward jet impingement effect, and introduced the sine of the impingement angle α , where $\alpha = (\alpha_1 + \alpha_2)/2$. The erosion depth variation $(E_{i2} - E_{j2})/l_2$ along the path appeared to be related to the combined effect of the vertical and horizontal jet impingements, and this was described in terms of the tangent of the impingement angle α . The erosion depth variation was found to have the same value as the change in the topographic incline angle represented by $\tan(\theta_0 - \beta)$. We thus obtained

$$E_{m2} = c * \frac{h_2}{d_m} * \frac{\gamma_2}{\gamma_{bed}} * v_2 * f_2(\sin \alpha) \quad (9)$$

$$\tan(\theta_0 - \beta) = \frac{E_{i2} - E_{j2}}{l_2} = d * \frac{h_2}{d_m} * \frac{\gamma_2}{\gamma_{bed}} * v_2 * f_4(\tan \alpha) \quad (10)$$

By simple deformation, Eqs. (6-7) respectively become

$$G = \frac{E_{m2}}{\frac{h_2}{d_m} * \frac{\gamma_2}{\gamma_{bed}} * v_2} = c * f_3(\sin \alpha) \quad (11)$$

$$H = \frac{\frac{E_{i2} - E_{j2}}{l_2}}{\frac{h_2}{d_m} * \frac{\gamma_2}{\gamma_{bed}} * v_2} = d * f_4(\tan \alpha) \quad (12)$$

Here again, the left sides of Eqs. (11-12) are respectively denoted by G and H . The variables G and H are shown as functions of their respective independent factors $\sin \alpha$ and $\tan \alpha$ in Figure 12 and 13.

From the above figures, we obtained $c = 0.01$ and $d = 5E-5$. The parameters c and d are experimental coefficients; the former is dimensionless while the latter has the dimension m^{-1} , and is a measure of the variation of the erosion depth in the sediment bed along the debris flow path. The two experimental coefficients reflect the effect of the impaction and impingement on the

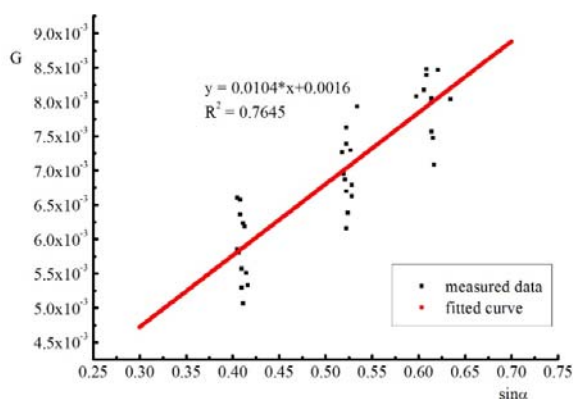


Figure 12 G as a function of sin α.

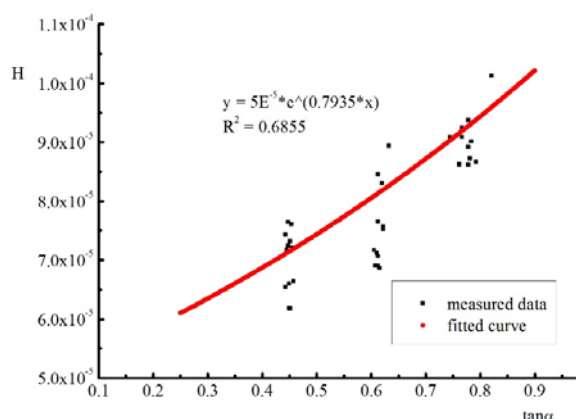


Figure 13 H as a function of tan α.

topographic concave site. By eliminating experimental errors, our proposed erosion equation becomes

$$E_{m2} = 0.01 * \frac{h_2}{d_m} * \frac{\gamma_2}{\gamma_{bed}} * v_2 * \sin \alpha \quad (13)$$

$$\tan(\theta_0 - \beta) = \frac{E_{j2} - E_{j2}}{l_2} = 5E^{-5} * \frac{h_2}{d_m} * \frac{\gamma_2}{\gamma_{bed}} * v_2 * e^{\tan \alpha} \quad (14)$$

As indicated in Table 2, the calculated Froude number *Fr* values are within 30–55, which means that the debris flows exhibited rapid flow features during their movement from the steep slope to the gentle slope. It was therefore reasonable to consider the high-speed debris flows that originated from the steep slope as jet impingements.

Hence, by our in-depth analysis of the entrainment processes in sections *AB* and *BC* of our flume experimental setup, we were able to obtain a rather clear understanding of the mechanics of the erosion of a sediment bed by a debris flow that travels over topographic inflexion

(convex and concave) points in the flow channel.

4 Discussion

As can be deduced from the equations proposed above, we assumed that the erosion rate was directly proportional to the bulk density of the debris flow. Because the bulk density in our experiments was always within the values for a dilute debris flow, the rationality of the proportional relationship between these two parameters was maintained. However, as noted by Takahashi (1991), the debris flow velocity depends not only on the channel gradient, but also on the concentration of the solid particles; the denser the concentration, the slower the velocity. He suggested that a fully developed debris flow no longer had bed eroding ability, neither could it grow, even along a steeply descending slope. Fagents (2006) also observed a decrease in the rate of entrainment with increasing density of a debris flow. This was attributed to bulking, which is the progressive damping of the turbulence of a debris flow as it assimilates sediments. Fagents (2006) thus proposed an upper limit ρ_{max} of the flow bulk density ρ , beyond which entrainment ceases.

The erodible bed in our experiment was composed of relatively loose and dry sediments. In addition, the duration of the release of the debris mixture from the hopper was rather short. We thus ignored permeation into the contact surface and the variation of the pore pressure in the sediment material. Consequently, the overriding debris flow was considered as a single-phase flow. However, in natural channels, loose materials are susceptible to rainfall and permeation increases the bed water content, resulting in secondary compaction and reduction of the overall stability, which consequently enhance mass erosion. Further study is thus required to establish the effects of the water content and compaction of loose materials on the mass erosion process at a topographic convex point along the channel.

5 Conclusions

Traditional equations of the erosion rate of a debris flow mostly apply to entrainment on a

relatively gentle slope along the channel. Together with the mass and momentum conservation equations, they can be used to simulate the evolution of the debris flow channel and obtain ideal results. However, when there are topographic inflexion points formed by plentiful loose materials along the flow path, the traditional equations may be inapplicable.

In our study, we identified two types of topographic points that affect the entrainment behavior of debris flow, namely, convex and concave points. At a topographic convex point, the entrainment process mainly manifests as mass erosion of the erodible bed and is dominated by external dynamic factors and the overall internal stability and strength of the bed sediments. We found an exponential relationship between the mass erosion intensity and the ratio of the bed slope angle to the friction angle. The relationship implies faster sharpening and planation of the bed with increasing steepness of the slope, and hence easier mass erosion. Conversely, when a debris flow passes over a topographic concave point, the erosion mainly occurs on the gentler downstream slope and behaves more like an impacting and impinging erosion rather than a traditional hydraulic erosion. The maximum erosion depth and outflow exit angle are significantly determined by the impact angle α_2 of the debris flow. The

maximum erosion depth is apparently proportional to $\sin \alpha_2$ while the outflow exit angle is correlated to $\tan \alpha_2$ in an exponential way. However, in the extreme case of an impact angle of 90° or 0° , neither the linear nor the exponential law is actually applicable.

In our experiments, we ignored permeation into the contact surface and variation of the pore pressure in the sediment material. The overriding debris flow was thus considered as a single-phase flow. However, in a real channel, loose materials are susceptible to rainfall and permeation increases the bed water content, resulting in secondary compaction and reduction of the overall stability. This enhances mass erosion. Further study is thus required to establish the effects of the water content and compaction of loose materials on the mass erosion process at convex sites.

Acknowledgements

This study was funded by the Key Research Program of the Chinese Academy of Sciences (Grant No. KZZD-EW-05-01), the National Natural Science Foundation of China (Grant No. 41371039), and the Open Foundation of State Key Laboratory of Hydraulics and Mountain River Engineering, Sichuan University (Grant No. SKHL1426).

References

- Beltaos S, Rajaratnam N (1973) Plane turbulent impinging jets. *Journal of Hydraulic Research* 11(1): 29-59.
- Brufau P, Garcia-Navarro P, Ghilardi P, et al. (2000) 1D mathematical modelling of debris flow. *Journal of Hydraulic Research* 38(6): 435-446. DOI: 10.1080/00221680009498297
- Cannon SH, Kirkham RM, Parise M (2001) Wildfire-related debris-flow initiation processes, Storm King Mountain, Colorado. *Geomorphology* 39: 171-188. DOI: 10.1016/S0169-555X(00)00108-2
- Coe JA, Kinner DA, Godt JW (2008) Initiation conditions for debris flows generated by runoff at Chalk Cliffs, central Colorado. *Geomorphology* 96: 270-297. DOI: 10.1016/j.geomorph.2007.03.017
- Tang C, Van Asch TW, Chang M, et al. (2012) Catastrophic debris flows on 13 August 2010 in the Qingping area, southwestern China: the combined effects of a strong earthquake and subsequent rainstorms. *Geomorphology* 139: 559-576. DOI: 10.1016/j.geomorph.2011.12.021
- Cui P, Zou Q, Xiang LZ, et al. (2013) Risk assessment of simultaneous debris flows in mountain townships. *Progress in physical geography* 37(4): 516-542. DOI: 10.1177/0309133313491445
- Egashira S, Honda N, Itoh T (2001) Experimental study on the entrainment of bed material into debris flow. *Physics and Chemistry of the Earth, Part C: Solar, Terrestrial & Planetary Science* 26(9): 645-650. DOI: 10.1016/S1464-1917(01)00062-9
- Fagents SA, Baloga SM (2006). Toward a model for the bulking and debulking of lahars. *Journal of Geophysical Research: Solid Earth* (1978-2012) 111(B10). DOI: 10.1029/2005JB003986.
- Godt JW, Coe JA (2007) Alpine debris flows triggered by a 28 July 1999 thunderstorm in the central Front Range, Colorado. *Geomorphology* 84: 80-97. DOI: 10.1016/j.geomorph.2006.07.009
- Hungr O, McDougall S, Bovis M (2005) Entrainment of material by debris flows. In *Debris-flow hazards and related phenomena* (pp. 135-158). Springer Berlin Heidelberg.
- Hu K, Cui P, Zhang J (2012) Characteristics of damage to buildings by debris flows on 7 August 2010 in Zhouqu, Western China. *Natural Hazards and Earth System Sciences* 12(7): 2209-2217.
- Iverson RM, Reid ME, Logan M, et al. (2011) Positive feedback and momentum growth during debris-flow entrainment of

- wet bed sediment. *Nature Geoscience* 4(2): 116-121. DOI: 10.1038/ngeo1040
- Iverson RM (2012) Elementary theory of bed - sediment entrainment by debris flows and avalanches. *Journal of Geophysical Research: Earth Surface* (2003–2012) 117: F03006. DOI: 10.1029/2011JF002189
- Khattak GA, Owen LA, Kamp U, et al. (2010) Evolution of earthquake-triggered landslides in the Kashmir Himalaya, northern Pakistan. *Geomorphology* 115: 102-108. DOI: 10.1016/j.geomorph.2009.09.035
- King J (1996) Tsing Shan Debris Flow (Special Project Report SPR 6/96,133pp.) Geotechnical Engineering Office, Hong Kong Government.
- Koi T, Hotta N, Ishigaki I, et al. (2008) Prolonged impact of earthquake-induced landslides on sediment yield in a mountain watershed, the Tanzawa region, Japan. *Geomorphology* 101: 692-702. DOI: 10.1016/j.geomorph.2008.03.007
- Lin CW, Liu SH, Lee SY, et al. (2006) Impacts on the Chi-Chi earthquake on subsequent rain-induced landslides in central Taiwan. *Engineering Geology* 86: 87-101. DOI: 10.1016/S0013-7952(03)00125-X
- Lin GW, Chen H, Chen YH, et al. (2008) Influence of typhoons and earthquakes on rainfall-induced landslides and suspended sediments discharge. *Engineering Geology* 97: 32-41. DOI: 10.1016/j.enggeo.2007.12.001
- Mazurek KA, Rajaratnam N, Sego DC (2003) Scour of a cohesive soil by submerged plane turbulent wall jets. *Journal of hydraulic research* 41(2): 195-206. DOI: 10.1080/00221680309499961
- Rajaratnam N (1981) Erosion by plane turbulent jets. *Journal of hydraulic Research* 19(4): 339-358. DOI: 10.1080/00221688109499508
- Sassa K, Kaibori M, Kitera N (1985) Liquefaction and undrained shear of torrent deposits as the cause of debris flows. In: Takei A. (ed.) *Proceedings of the International Symposium on Erosion, Debris Flows and Disaster Prevention* The Erosion-control Engineering Society, Japan, Tokyo. pp: 231-236
- Shieh CL, Jan CD, Tsai YF (1996) A numerical simulation of debris flow and its application. *Natural Hazards* 13(1): 39-54. DOI: 10.1007/BF00156505
- Suzuki T, Miyamoto K (2009) Numerical simulation method of debris flow introducing the non-entrainment erosion rate equation, at the transition point of riverbed gradient or the channel width and in the area of sabo dam. *Journal of the Japan Society of Erosion Control Engineering* 62(3): 14-22.
- Takahashi T (1978) Mechanical characteristics of debris flow. *Journal of the Hydraulics Division* 104(8): 1153-1169.
- Takahashi T (1991) *Debris Flow*. IAHR Monograph. A. A. Balkema, Rotterdam.
- Takahashi T, Kuang SF (1986) Formation of debris flow on varied slope bed. *Annuals Disaster Prevention Research Institute, Kyoto Univ.* 29B-2: 343-359.
- Tang C, Rengers N, Van Asch TW, et al. (2011) Triggering conditions and depositional characteristics of a disastrous debris flow event in Zhouqu city, Gansu Province, northwestern China. *Natural Hazards and Earth System Science* 11(11): 2903-2912. DOI: 10.5194/nhess-11-2903-2011
- Wang G, Sassa K, Fukuoka H (2003) Downslope volume enlargement of a debris slide-debris flow in the 1999 Hiroshima, Japan, rainstorm. *Engineering Geology* 69: 309-330. DOI: 10.1016/S0013-7952(02)00289-2